JOURNAL OF MATERIALS SCIENCE 11 (1976) 801–808

Phase equilibria and transformations in the system Li_2GeO_3-Na_2GeO_3

A. R. WEST, A. J. BLAKE
Department of Chemistry, University of Aberdeen, Meston Walk, Old Aberdeen, Aberdeen, UK

The phase diagram has been determined using a combination of high temperature powder diffraction and quench furnace equilibration. Na_2GeO_3 forms a range of solid solutions which covers over half of the diagram at solidus temperatures (900° C) but whose extent is much more restricted at lower temperatures. Na_2GeO_3 solid solutions may undergo a variety of reactions on cooling, which include phase transformation and coherent precipitation.

1. Introduction

The present report forms part of a study on synthetic complex oxide systems which contain two alkali metal ions. In an earlier study of the silicate system Na_2SiO_3–Li_2SiO_3, extensive solid solution formation was found at high temperatures and various transformation reactions occurred during cooling of these solid solutions [1]. An interesting observation was the occurrence of a range of solid solutions which apparently had a modulated superstructure and whose modulation wavelength varied with composition [2]. It was felt that the corresponding germanate system might also show interesting solid solution effects. The end-member phases Na_2GeO_3 and Li_2GeO_3 are both well-known [3, 4], but reactions between them have not been studied previously. Li_2GeO_3 is isostructural with Li_2SiO_3 and Na_2SiO_3 [5–7]. Its structure can be thought of either as (i) a distorted wurtzite superstructure, with hexagonal close packed oxygen and cations ordered on one set of distorted tetrahedral sites, or as (ii) a $(GeO_3)_\infty$ "Zweiereinfachketten" chain structure.

2. Experimental

Starting materials were Li_2CO_3, Na_2CO_3 (both reagent grade) and GeO_2 (electronic grade). Compositions (1 to 2 g each) were mixed into a paste with acetone, dried, and fired in Pt crucibles in electric muffle furnaces, initially at 600° C to drive off CO_2, and finally at 800 to 850° C for 1 to 3 days. Completeness of reaction was checked using Guinier X-ray powder methods.

Two techniques were used to determine the phase diagram. (1) Small samples (about 50 mg) of the reacted compositions were wrapped in Pt foil and suspended in conventional, vertical tube quench furnaces for times ranging from 2 h to 3 days. Runs were terminated by dropping the samples into a dish of mercury. The furnace was calibrated at the gold point (1063° C); measured temperatures are accurate to ±4° C. The quenched samples were examined by optical microscopy as well as by X-ray methods. (2) Small samples (10 to 20 mg) were mounted on a Pt gauze and their powder patterns taken at high temperatures with a continuously-recording Nonius Guinier–Lenne camera. This method was particularly useful for determining the limits of the solid solution fields and also as a check on melting behaviour at the solidus. Temperatures of phase transitions, phase boundaries etc, as determined by this method, are accurate to ±25° C.

An attempt was made to use DTA to study the subsolidus equilibria. However, it was found that the heating and cooling rates used (about 20° C min^{-1}) were much too rapid for equilibrium to be followed without considerable hysteresis; in addition, metastable side reactions occurred which complicated the DTA traces.

3. Results and discussion

3.1. The phase diagram

Using the combined techniques of quench furnace equilibration and high temperature powder diffraction, the equilibrium diagram shown in Fig. 1 was constructed. The system is binary at all temperatures. A large range of solid solutions extends from Na_2GeO_3 to 57 ± 2% Li_2GeO_3* at solidus temperatures. The liquidus curve above these solid solutions passes through a thermal minimum at 42 ± 6% Li_2GeO_3 and 895 ± 6° C and the most lithium-rich member of these solid solutions melts incongruently to Li_2GeO_3 solid solution (ss) plus liquid at 914 ± 7° C.

The liquidus relations are shown dashed for the most part because quantitative data were difficult to obtain. There is very little tendency to glass formation in melts of this system. Thus, although glass was observed in some samples (of compositions near to the thermal minimum) which had been quenched rapidly from above solidus temperatures, it was difficult to prepare specimens of pure glass, even by quenching from temperatures which must have been well above the liquidus for those compositions. If slightly slower cooling rates were used, such as cooling the samples by blowing on them rather than by dropping them into mercury, no glass was generally observed.

The solidus temperatures were determined mainly from a comparison of the results of sets of identical equilibration runs on samples of different composition (often two or three samples were heated concurrently in the same furnace). The physical appearance of the samples was assessed—loose powder, glazed film, etc—and a microscope study was made of textures, crystal quality (extinction) and the occurrence of glass.

The subsolidus equilibria were studied most reliably from high temperature powder X-ray photographs. The solvus curve limiting the compositional extent of the Na_2GeO_3 solid solutions was determined by noting the temperature at which Li_2GeO_3 was observed to appear in the X-ray photographs on the cooling cycle. The reverse reaction, dissolution of Li_2GeO_3 by Na_2GeO_3 ss, was followed on the heating cycle for a few compositions in order to check that the temperatures obtained on cooling had not been reduced significantly by hysteresis. As shown in Fig. 1, the extent of the Na_2GeO_3 solid solution field undergoes a dramatic contraction with falling temperature. Li_2GeO_3 forms a much more restricted range of solid solutions, dissolving a maximum of 17 ± 5% Na_2GeO_3 at the solidus. There is a close similarity between Fig. 1 and the phase diagram of the corresponding silicate system, Li_2SiO_3–

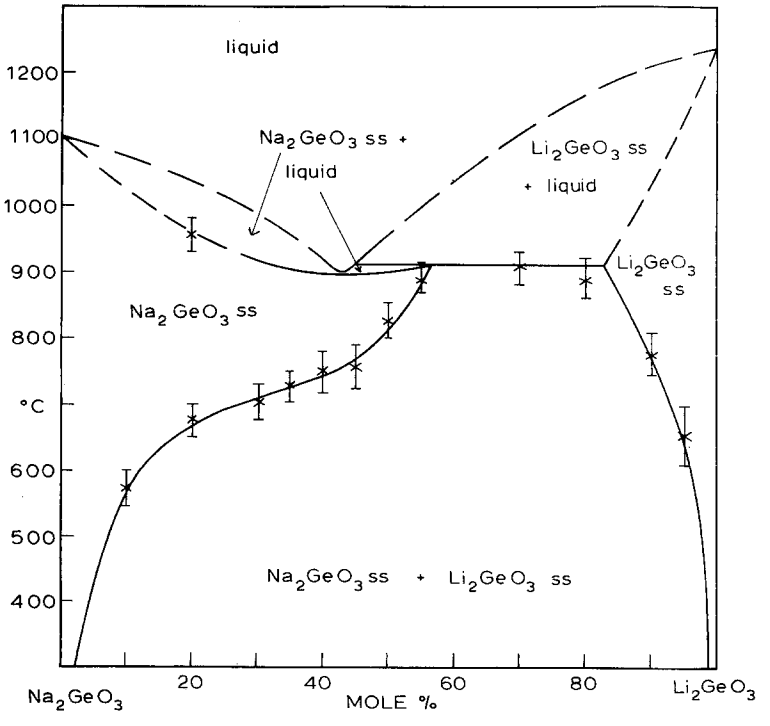

Figure 1 Equilibrium phase diagram for the system Na_2GeO_3–Li_2GeO_3. The data points marked are those determined by high temperature powder diffraction.

* All percentages are mol %.

Na_2SiO_3 [1]. In the germanates, the Na_2GeO_3ss field extends some 4% further at the solidus than that of Na_2SiO_3ss, and melting temperatures are generally about 50° C higher.

The variation of unit cell parameter with solid solution composition at 800° C was determined from high temperature powder photographs and is shown in Fig. 2. Powder lines from the Pt gauze sample holder acted as an internal standard and for this purpose the *d*-spacings of the first four Pt lines at 800° C were calculated to be 2.28, 1.98, 1.40 and 1.19 Å (using a coefficient of linear expansion for Pt of 1×10^{-5}). The *d*-spacings of the (0 0 2) and the overlapping (2 0 0) and (1 3 0) lines of the solid solutions were then measured and from these, cell dimensions were calculated. The solid solutions are presumably formed by disordering of Na and Li over the alkali ion sites; from Fig. 2 the cell parameters change smoothly but non-linearly with composition and so Vegard's Law is not obeyed. It was not possible to determine the variation of cell parameters with composition at room temperature, because most of the (Na_{2-x}, Li_x) GeO_3 solid solutions decomposed, even on rapid cooling (see later).

Indexed powder diffraction patterns for Li_2GeO_3 and Na_2GeO_3 are given in Table I and unit cell dimensions determined from the refined powder data in Table II. The data were recorded with a Philips Hägg Guinier camera using Cu$K\alpha$ radiation, and KCl ($a_0 = 6.2931$ Å) was added as an internal standard. These new data show many more lines than are given in the literature [3, 4, 8] and the latter data are either unindexed (Li_2GeO_3) or indexed on the wrong unit cell (Na_2GeO_3). The crystal structure of Li_2GeO_3 is known [5]; it is isostructural with Li_2SiO_3 and Na_2SiO_3 [6, 7]. Na_2GeO_3 also appears to be isostructural from its powder pattern, although single crystal studies to confirm this have not been carried out. Na_2GeO_3 is closer to being geometrically pseudohexagonal than is Li_2GeO_3 and most of the powder lines of Na_2GeO_3 could not be uniquely assigned with certainty.

One difficulty in working with Na_2GeO_3-rich compositions was that weak extra powder lines were sometines observed. These are most likely due to an impurity phase, possibly a previously unreported sodium germanate phase. The extra lines were usually absent from high temperature powder photographs taken on the cooling cycle over the range 800° C to room temperatures and so are not thought to represent a genuine feature of the Na_2GeO_3–Li_2GeO_3 system.

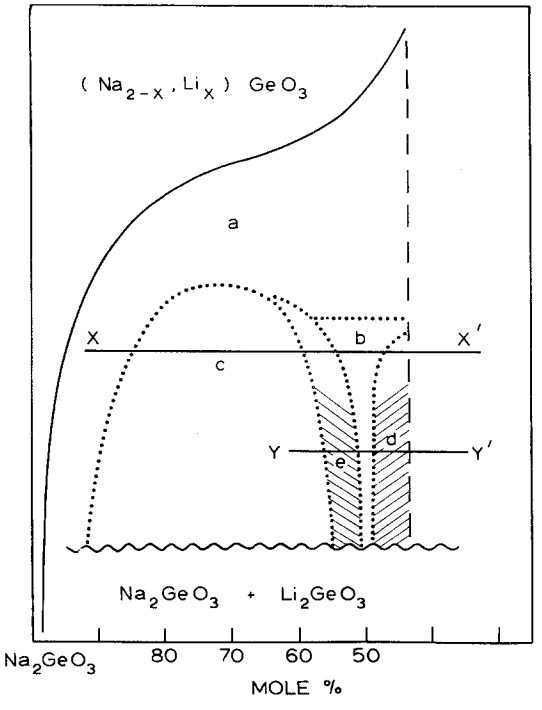

Figure 2 Variation of unit cell parameters with composition at 800° C.

3.2. Metastable phases and reactions

Although the equilibrium phase diagram is relatively simple, the behaviour of (Na_{2-x}, Li_x) GeO_3 solid solutions on cooling is complex and depends on both cooling rate and composition. With fairly slow cooling, e.g. from 800° C to room temperature in a few hours, an equilibrium pathway is followed yielding the assemblage ($Na_2GeO_3 + Li_2GeO_3$). However, with more rapid cooling rates, metastable products may be obtained. Fig. 3 summarizes schematically the phenomena which have been observed so far. Solid solutions containing $\gtrsim 10\%$ Li_2GeO_3 cannot usually be preserved intact to room temperatures, even on rapid quenching (section X–X′). Compositions around 50% Li_2GeO_3 transform to a metastable phase, low-(Na, Li)$_2GeO_3$ss (region b). Intermediate compositions (~15 to 40% Li_2GeO_3) decompose, to yield (Na_2GeO_3ss + low-(Na, Li)$_2GeO_3$ss) and it appears than an immiscibility dome occurs within the undercooled $(Na_{2-x}, Li_x)GeO_3$ solid solution (region c). Low-(Na, Li)$_2GeO_3$ appears to form a short range of solid solutions when prepared by rapid quenching and these solid solutions precipitate the excess Na_2GeO_3 and Li_2GeO_3 respectively,

TABLE I Powder diffraction data

d_{obs} (Å)	d_{calc} (Å)	I_{vis}	hkl
Li_2GeO_3			
4.81	4.81	80	0 2 0
4.76	4.76	60	1 1 0
3.40	3.39	100	1 1 1
2.77	2.77	60	1 3 0
2.739	2.739	40	2 0 0
2.418	2.418	40	0 0 2
2.406 b*	2.405	60	0 4 0
	2.402		1 3 1
2.381	2.383	20	2 0 1
	2.380		2 2 0
2.160	2.160	20	0 2 2
2.157	2.156	10	1 1 2
2.135	2.136	20	2 2 1
1.821	1.821	20	1 3 2
1.814	1.815	20	1 5 0
	1.813		2 0 2
1.807	1.807	5	2 4 0
1.793	1.794	20	3 1 0
1.706	1.705	10	0 4 2
1.699	1.700	20	1 5 1
	1.696		2 2 2
1.693	1.693	20	2 4 1
1.681	1.682	10	3 1 1
1.604	1.603	20	0 6 0
1.586	1.587	40	3 3 0
1.529	1.527	20	1 1 3
1.450	1.452	5	1 5 2
1.447	1.448	10	2 4 2
1.441	1.441	20	3 1 2
1.393	1.393	40	1 3 3
1.389	1.389	10	2 0 3
1.384	1.384	10	2 6 0
1.336	1.336	40	0 6 2
	1.335		2 2 3
	1.333		1 7 0
1.330	1.330	10	2 6 1
1.326	1.327	40	3 3 2
	1.325		3 5 0
1.317	1.318	10	4 0 1
	1.317		4 2 0
1.285	1.285	20	1 7 1
1.276	1.277	5	3 5 1
1.270	1.271	20	4 2 1
low-(Na, Li)$_2GeO_3$			
5.15	5.14	40	$\bar{1}$ 1 0
5.09	5.09	60	0 2 0
5.03	5.02	20	1 1 0
3.564	3.560	80	$\bar{1}$ 1 1
3.525	3.521	80	1 1 1
2.971	2.969	20	$\bar{1}$ 3 0
2.930	2.929	40	2 0 0
2.901	2.903	20	1 3 0
2.571	2.568	20	$\bar{2}$ 2 0
2.549	2.545	40	$\bar{1}$ 3 1
2.521	2.519	40	2 0 1
2.502	2.503	20	1 3 1
2.471	2.470	100	0 0 2
2.281	2.278	10	$\bar{2}$ 2 1

d_{obs}(Å)	d_{calc}(Å)	I_{vis}	hkl
low-(Na, Li)$_2GeO_3$ continued			
2.261	2.262	5	0 4 1
2.238	2.238	10	2 2 1
2.224	2.222	40	0 2 2
1.928	1.927	5	$\bar{3}$ 1 0
1.909	1.909	20	3 1 0
1.899	1.899	40	$\bar{1}$ 3 2
1.890	1.888	40	2 0 2
1.881	1.881	40	1 3 2
1.812	1.811	5	$\bar{2}$ 4 1
1.804	1.804	5	$\bar{1}$ 5 1
1.781	1.780	20	$\bar{2}$ 2 2
1.770	1.772	10	0 4 2
	1.770		2 4 1
1.713	1.712	20	$\bar{3}$ 3 0
1.693	1.696	10	0 6 0
1.671	1.674	40	3 3 0
1.568	1.568	40	$\bar{1}$ 1 3
	1.567		0 2 3
1.564	1.565	40	1 1 3
1.520	1.519	5	$\bar{3}$ 1 2
1.509	1.510	10	3 1 2
	1.510		1 5 2
1.485	1.485	5	$\bar{2}$ 6 0
1.464	1.465	5	4 0 0
1.441	1.440	40	$\bar{1}$ 3 3
1.436	1.435	40	2 0 3
1.432	1.432	20	1 3 3
1.421	1.422	5	2 6 1
	1.420		$\bar{1}$ 7 0
1.408	1.407	20	$\bar{3}$ 3 2
	1.404		4 0 1
1.397	1.398	20	0 6 2
	1.398		4 2 0
1.391	1.393	20	2 6 1
	1.391		3 5 0
1.385	1.386	40	$\bar{2}$ 2 3
	1.385		3 3 2
	1.382		0 4 3
1.372	1.372	5	$\bar{3}$ 5 1
1.362	1.365	10	$\bar{1}$ 7 1
	1.362		$\bar{4}$ 2 1
1.345	1.345	10	4 2 1
1.272	1.273	5	$\bar{2}$ 6 2
	1.272		0 8 0
1.256	1.257	10	$\bar{2}$ 4 3
	1.255		4 4 0
	1.255		$\bar{1}$ 5 3
Na_2GeO_3			
5.44	60	0 2 0, 1 1 0	
5.41	40		
3.64	100	1 1 1	
3.127	80	1 3 0, 2 0 0	
3.109	60		
2.640	80	1 3 1, 2 0 1	
2.629	60		
2.463	80	0 0 2	
2.366	40	2 2 1	
2.240	40	0 2 2, 1 1 2	

Table 1 continued

d_{obs} (Å)	d_{calc} (Å)	I_{vis}	hkl	d_{obs} (Å)	d_{calc} (Å)	I_{vis}	hkl
Na_2GeO_3 continued				*Na_2GeO_3 continued*			
2.050	40	150, 240, 310		1.560	10		
2.042	40			1.501	10		
1.937	80	132, 202		1.493	40		
1.935	40			1.487	20		
1.894	60	151, 241		1.459	20		
1.812	40	222, 060, 330		1.455	100		
1.802	80			1.441	20		
1.572	40			1.433	20		
1.567	10			1.405	20		

* b = broad.

on annealing at about 400° C. In the initial stages, the precipitates are coherent with the matrix (regions e and d, Fig. 3). The phenomena in regions b to d have been studied in some detail and are described below.

3.2.1. Low-(Na, Li)$_2GeO_3$

The composition 50% Li_2GeO_3 is not a special composition as regards the Na_2GeO_3ss field; it is merely one member of the solid solution series. However, a stoichiometric metastable phase, low-(Na, Li)$_2GeO_3$, can be prepared by cooling the high temperature solid solution fairly quickly (850° C to room temperature in about 1 to 20 secs). At these cooling rates, the equilibrium precipitation of Li_2GeO_3ss is bypassed and the

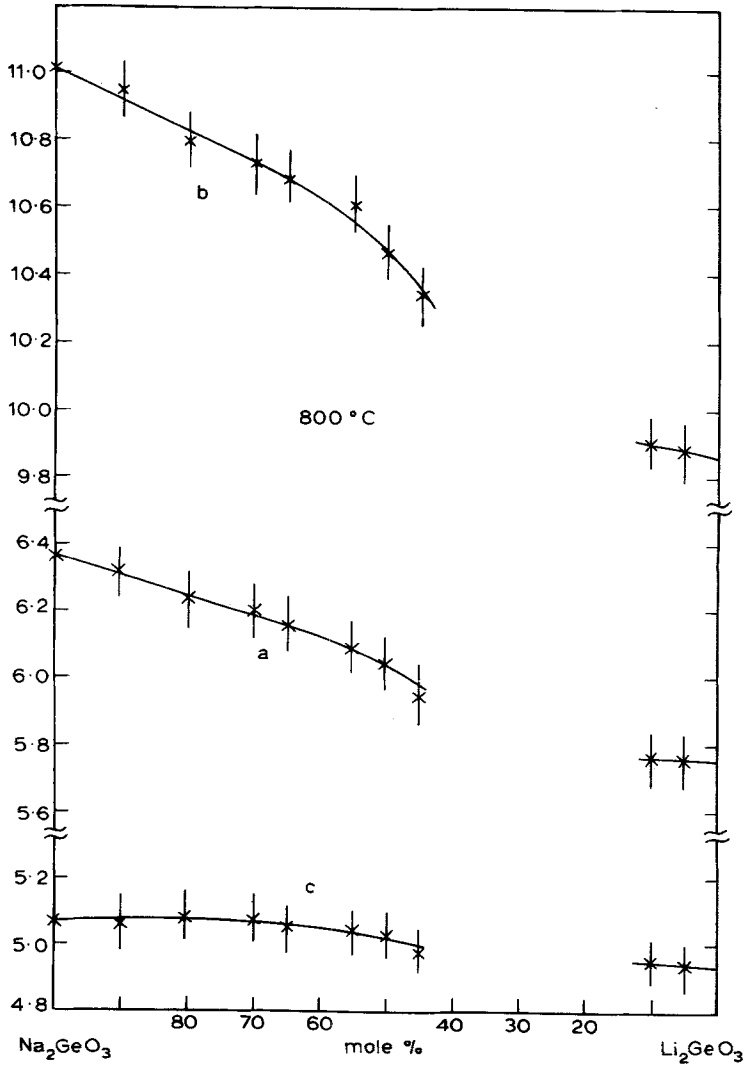

Figure 3 Schematic representation of the metastable phases and reactions which have been observed on cooling Na_2GeO_3 solid solutions. The vertical axis is a combination of temperature and cooling rate. (a) undercooled single phase solid solution; (b) low-(Na, Li)$_2GeO_3$ss; (c) metastable two-phase assemblage Na_2GeO_3ss + matrix; (e) Na_2GeO_3 precipitate coherent with low-(Na, Li)$_2GeO_3$ matrix. Section X–X′ represents the products of rapid quenching (850° C to 25° C in ~1 sec). Y–Y′ represents the products of rapid quenching followed by annealing at ~400° C.

TABLE II Crystallographic data

Phase	Symmetry	a (Å)	b (Å)	c (Å)	Reference
Li_2GeO_3	orthorhombic	9.63_0	5.46_5	4.85_0	[5]
Li_2GeO_3	orthorhombic	5.47_8	9.62_0	4.83_6	this work
Na_2GeO_3	orthorhombic	6.21_8	10.88_0	4.92_6	this work
low-(Na, Li)$_2GeO_3$	monoclinic $\gamma = 91.5 \pm 0.5°$[a]	5.86 ± 0.01	10.18 ± 0.02	4.94 ± 0.01	this work
Li_2SiO_3	orthorhombic	5.39_2	9.39_6	4.66_0	[1]
Na_2SiO_3	orthorhombic	6.07	10.48	4.82	[6]
low-(Na, Li)$_2SiO_3$	monoclinic $\gamma = 91.5 \pm 0.5°$[a]	5.73	9.86	4.77	[1]

[a] Not the smallest unit cell, but chosen for simplicity.

undercooled solid solution experiences a phase transition. Low-(Na, Li)$_2GeO_3$ apparently forms a short range of solid solutions on either side of the ideal composition but these solid solutions decompose on annealing to yield low-(Na, Li)$_2GeO_3$ and either Na_2GeO_3 or Li_2GeO_3. By DTA, low-(Na, Li)$_2GeO_3$ transforms to the undercooled high temperature solid solution at 654° C (642° C on cooling). The timescale of the DTA experiment, with a quick change from heating to cooling cycles at about 680° C, was sufficiently rapid for the transition to be observed before much decomposition to the equilibrium assemblage of (Na_2GeO_3ss + Li_2GeO_3ss) had occurred (as confirmed by the powder photograph of the sample taken after DTA). The transition: low-(Na, Li)$_2GeO_3$ $\rightleftharpoons$ undercooled solid solution, could not be observed directly by high temperature powder diffraction because 1 to 2 h are required to take an exposure and decomposition of low-(Na, Li)$_2GeO_3$ to the equilibrium assemblage occurred within this time at about 600 to 650° C. However, the occurrence of low-(Na, Li)$_2GeO_3$ is analogous to that of a corresponding meta-silicate phase, low-(Na, Li)$_2SiO_3$, and in the latter case the low- high transition was observed by high temperature powder diffraction [1].

From single crystal X-ray photographs, low-(Na, Li)$_2GeO_3$ is monoclinic. It is structurally related to the orthorhombic high temperature solid solution as its powder pattern is derived from that of the latter simply by the splitting of certain lines. For the purpose of indexing the powder pattern and in order to indicate the close similarity to the high temperature structure, a monoclinic unit cell has been chosen which is a slight distortion ($\gamma = 91.5°$) of the orthorhombic cell. However, this cell, which is C-centred with c as the unique axis, does not meet space group requirements and a smaller, primitive monoclinic cell should be chosen for correctness. Crystals of low-(Na, Li)$_2GeO_3$ were twinned with the bc plane of the C-centred cell as the twinning plane. On e.g. $(hk0)$ precession photographs, the twinning was observed as the doubling of spots along a^*; the magnitude of these spot separations increased as k (or $|\bar{k}|$) increased (no splitting observed for $k = 0$). Powder data for low-(Na, Li)$_2GeO_3$ are given in Table I and unit cell parameters in Table II. Also included in Table II, for comparison purposes, are literature data for the sodium, lithium metasilicates.

3.2.2. Decomposition of (Na_{2-x}, Li_x)GeO_3 solid solutions during cooling ($0.3 \lesssim x \lesssim 0.8$)

Na_2GeO_3 solid solutions of intermediate composition decompose, even on rapid quenching (~1 sec), into two phases which are approximately Na_2GeO_3 and low-(Na, Li)$_2GeO_3$. The compositions of these products are uncertain because the powder patterns are of poor quality with some diffuse and streaked lines. The rapidity of this decomposition reaction, together with the relative flatness of the Na_2GeO_3 ss solvus curve in this composition range (Fig. 1) points to the occurrence of an immiscibility gap or spinodal within the undercooled solid solutions. It was hoped to study this decomposition reaction on DTA cooling cycles and perhaps to plot out the position of an immiscibility dome. However, the DTA cooling rates were too slow to prevent some decomposition to the equilibrium assemblage of (Na_2GeO_3ss + Li_2GeO_3ss) from occurring, and so the DTA traces, which were quite complex, could not be interpreted unambiguously. Precession photographs of a "single crystal" of composition 30% Li_2GeO_3, quenched from 890° C, showed the presence of two phases, Na_2GeO_3 and low-(Na, Li)$_2GeO_3$ (approximate compositions) in very similar orientations: corresponding unit cell axes were parallel to within ±1 to 2°. However, the

photographs were of poor quality. Na_2GeO_3 spots were rather diffuse and the low-(Na, Li)$_2GeO_3$ spots were multiple (in addition to the doubling arising from twinning).

It is an interesting observation that the metastable immiscibility dome (assuming that it exists) has, as one of its members, (Na, Li)$_2GeO_3$ and not Li_2GeO_3. This is presumably for a combination of structural and kinetic reasons. First, low-(Na, Li)$_2GeO_3$ does have some stability and can be easily prepared, although it does not appear on the equilibrium phase diagram. Second, in the initial stages of decomposition the products as well as having similar orientations, are probably connected by a coherent interface. The stresses due to differences in volume of the phases on either side of the interface will be considerably less for Na_2GeO_3/(Na, Li)$_2GeO_3$ than for Na_2GeO_3/Li_2GeO_3. Hence, the initial decomposition to (Na, Li)$_2GeO_3$ + Na_2GeO_3 should have a lower activation energy than decomposition to the equilibrium assemblage, $Na_2GeO_3 + Li_2GeO_3$.

3.2.3. Precipitation of Li_2GeO_3 from low-(Na, Li)$_2GeO_3$ss

The phase low-(Na, Li)$_2GeO_3$ can apparently be prepared with an excess of Li_2GeO_3 in solid solution, as shown by quenching composition 55% Li_2GeO_3 from about 890° C. The product of such experiments was single-phase by X-ray diffraction but its powder pattern was virtually identical to that of low-(Na, Li)$_2GeO_3$; no shifts in *d*-spacing could be detected. On annealing this quenched material at 300 to 600° C, a small amount of Li_2GeO_3 was precipitated, but at the lower annealing temperatures, ~400 to 480° C, the Li_2GeO_3 phase had an anomalous powder pattern. The powder lines were generally broad and diffuse and were shifted slightly, usually to higher *d*-spacing compared with "normal" Li_2GeO_3. In addition, small variations in powder pattern occurred from sample to sample, notably with the (1 1 1) reflection which was sometimes split. This splitting could possibly be due to the appearance of (0 2 1) which is normally a systematically absent reflection but is more likely due to a monoclinic distortion causing the separation of (1 1 1) and ($\bar{1}$ 1 1) reflections.

Single crystal X-ray studies of material annealed at 400° C showed that the crystallographic axes of the Li_2GeO_3 precipitate were accurately aligned (to within 1° or better) with the corresponding pseudo-orthorhombic axes of low-(Na, Li)$_2GeO_3$. The Li_2GeO_3 spots were all uniformly somewhat diffuse. The unit cell dimensions of Li_2GeO_3 could not be determined with sufficient accuracy from precession photographs to confirm the small differences between normal and anomalous Li_2GeO_3 observed in Guinier powder photographs.

The most likely cause of the anomalous Li_2GeO_3 powder pattern is that the Li_2GeO_3 precipitate is coherent or partly coherent with the (Na, Li)$_2GeO_3$ matrix. In the earliest stages, perhaps in the as-quenched material, zoning probably occurs giving a non-random solid solution. On annealing, these zones form discrete precipitates but the precipitate/matrix interface is still continuous. Coherency stresses could account for both the *d*-spacing shifts ("stretching" of the Li_2GeO_3 structure) and the splitting of the (1 1 1) reflection (to match the monoclinic symmetry of the low-(Na, Li)$_2GeO_3$ matrix). The observed line broadening is probably a combination of coherency strains and small particle size.

3.3. General comments

Solid solutions formed by Na $\rightleftharpoons$ K replacement are common, e.g. in the feldspars. However, the difference in size of Na^+ and Li^+ is normally too great for extensive solid solutions to form by Na $\rightleftharpoons$ Li substitution. In the present system, Na_2GeO_3 forms extensive solid solutions but only at high temperatures, and most of these solid solutions decompose very quickly during cooling.

Several stages in the decomposition of the solid solutions have been identified. There is indirect evidence of the occurrence of a spinodal within the metastable, undercooled solid solutions. Decomposition is very rapid within this spinodal and proceeds more or less to completion with cooling rates as high as 200 to 500° C sec^{-1}. Hence X-ray side bands, which are generally observed in the early stages of spinodal decomposition, were absent from the present materials. One example of coherent precipitation, that of Li_2GeO_3 from low-(Na, Li)$_2GeO_3$ss, has been studied in some detail. Other examples could probably be found; e.g. precipitation of low-(Na, Li)$_2GeO_3$ from an Na_2GeO_3 solid solution which has a composition just to the Na_2GeO_3-rich side of the spinodal. These coherent reactions are made possible by (a) the structural similarity of the phases Na_2GeO_3, low-(Na, Li)$_2GeO_3$ and Li_2GeO_3 and (b) by their not too dissimilar unit cell dimensions.

During an earlier study of the corresponding metasilicate system, a modulated superstructure was found in compositions around 50% Na_2SiO_3 [2]. This phase apparently formed as an intermediate during the conversion: high temperature solid solution → modulated superstructure → low-$(Na, Li)_2SiO_3$ss. With the metagermanate solid solutions, it was not generally possible to suppress the transformation to low-$(Na, Li)_2GeO_3$ss with the quenching rates available. Hence it is not known whether a modulated superstructure is also possible in this system.

References

1. A. R. WEST, *J. Amer. Ceram. Soc.*, in press.
2. A. R. WEST, in preparation.
3. M. K. MURTHY and J. AGUAYO, *J. Amer. Ceram. Soc.* 47 (1964) 444.
4. M. K. MURTHY and J. IP, *ibid* 47 (1964) 328.
5. H. VÖLLENKLE and A. WITTMAN, *Monat. Chem.* 99 (1968) 244.
6. W. S. MCDONALD and D. W. CRUICKSHANK, *Acta Cryst.* **22** (1967) 37.
7. H. SEEMAN, *ibid* 9 (1956) 251.
8. ASTM Powder Diffraction File, Card No. 18-1217.

Received 10 October and accepted 11 November 1975.